INTERNATIONAL JOURNAL FOR NUMERICAL METHODS IN FLUIDS
Int. J. Numer. Meth. Fluids 2006; **50**:1321–1334
Published online 20 December 2005 in Wiley InterScience (www.interscience.wiley.com). DOI: 10.1002/fld.1143

Three-dimensional lattice Boltzmann BGK model and its application to flows with heat transfer in a rectangular microchannel

Y. T. Chew*,†, X. D. Niu‡ and C. Shu§

Department of Mechanical Engineering, National University of Singapore, Singapore 117576, Singapore

SUMMARY

In this paper, we present a 3D lattice Boltzmann BGK model for simulation of micro flows with heat transfer. This model is an extension of the two-dimensional model that is based on the kinetic theory and the thermal lattice Boltzmann method. The kinetic relations of the relaxation times in this model were linked with the Knudsen number, and a diffuse scattering boundary condition for the velocity and thermal fields was presented for the 3D lattice Boltzmann method. The present 3D lattice Boltzmann model was successfully applied to simulate the flow and heat transfer in rectangular channels using the 3D TLLBM developed by the authors. Numerical results obtained by the present method show that the LBM can give a good prediction of the micro fluidic behaviours with thermal effects. Copyright © 2005 John Wiley & Sons, Ltd.

KEY WORDS: 3D lattice Boltzmann; micro flows; heat transfer

INTRODUCTION

The rapid development of micro electromechanical systems (MEMS) has resulted in an increasing demand for highly efficient electronic cooling technologies [1, 2]. To meet this demand, a deep understanding of the flow and heat transfer in micro scale is important. To date, extensive numerical and experimental studies on this topic have been carried out by many authors [3–8]. However, most numerical works are based on solving the continuum Navier–Stokes (N–S) and energy equations. Theoretically, since the size of a device is of

*Correspondence to: Y. T. Chew, Department of Mechanical Engineering, National University of Singapore, Singapore 117576, Singapore.
†E-mail: mpecyt@nus.edu.sg
‡E-mail: mpenxd@nus.edu.sg
§E-mail: mpeshuc@nus.edu.sg

Received 15 March 2005
Revised 18 October 2005
Accepted 30 October 2005

micro scale, the continuum flow assumption is no longer valid because the characteristic length of the flow is of comparable order of magnitude of the mean free path λ and the inter-molecular interactions are manifested. The microscopic flows are usually characterized by a dimensionless parameter—the Knudsen number $Kn = \lambda/H$ (H is the characteristic length scale of the flow). When $Kn \geqslant 0.01$, the flow is considered to be in the slip ($0.01 < Kn \leqslant 0.1$) flow, transition ($0.1 < Kn \leqslant 10$) or free molecular ($Kn > 10$) regime according to the ranges of Knudsen number. Numerical studies of these kinds of flows should be based on the solution of full Boltzmann equation (BE) [9–11], or the particle methods involving molecular dynamics (MD) [12], or the direct simulation Monte Carlo (DSMC) method [13]. However, the computational effort of the MD and the DSMC methods is usually huge even with the use of most powerful supercomputer, and the schemes used for solving the full BE are complicated because they require the integration of a six-independent-variables function.

Recently, the lattice Boltzmann method (LBM) has received considerable attention by fluid dynamic researchers [14, 15]. The LBM is designed to solve the lattice Boltzmann equation (LBE) kinetically on a regular lattice where a number of fictitious particles evolve according to the laws pertaining to the basic fluid principles of mass, moment and energy conservation. Unlike the MD and DSMC methods, the number of particles distributed in the computational field in the LBM is not related to the number of molecules. Therefore, the LBM is computationally more efficient than the MD and DSMC methods. Furthermore, since the LBM solver is based on a simple BGK collision approximation [16], one avoids solving complicated schemes needed for the full BE. Besides, the LBM is intrinsically kinetic since the BGK collision approximation essentially represents the physics of molecular interactions, and the equilibrium distribution function in the approximation can be considered as an effective equilibrium of the molecular motions. Hence it has a strong theoretical foundation to be taken as an alternative simpler means to model the microscopic fluid dynamics problems.

In this paper, we present a three-dimensional (3D) lattice Boltzmann BGK model for simulating the micro flow with heat transfer. This 3D model is an extension of the two-dimensional model [17] that is based on the classic kinetic theory [18] and the thermal lattice Boltzmann method (TLBM) [19]. The TLBM has been shown capable of simulating thermal flow with arbitrary Prandtl numbers by defining density and internal energy density distribution functions separately with their respective relaxation times representing hydrodynamic and thermodynamic fields [19]. The difference between the present 3D model and the 2D model proposed in Reference [17] is that the relaxation times are redefined and linked to the Knudsen number based on the kinetic theory [18] and hard sphere assumption [9, 20]. Besides, in consistency with the kinetic theory, a diffuse-scattering boundary condition (DSBC) for the 3D LBM is presented in this paper according to our previous work [17] so that the velocity slips and temperature jumps at walls are captured correctly.

To verify the present 3D lattice Boltzmann BGK model, a developing thermal flow in a rectangular microchannel with different aspect ratios is studied using our Taylor series expansion and least square-based LBM (TLLBM) [21] which can be applied on non-uniform grids. The TLLBM is a meshless method and has been proven to be an efficient and accurate solver for simulating the continuum flows [22, 23]. The results obtained by present LBM are compared with those of Tunc and Bayazitoglu [24] and the DSMC method [25]. Their works are based on solutions of the traditional momentum and energy equations with first-order velocity slip and temperature jump conditions.

3D THERMAL LATTICE BOLTZMANN MODEL FOR MICROFLUIDICS

The thermal lattice Boltzmann equation with BGK model [17] is derived from the kinetic theory and can be written as

$$\overline{f_\alpha}(\mathbf{r}+\mathbf{e}_\alpha\delta_t, t+\delta_t) = \overline{f_\alpha}(\mathbf{r},t) + \frac{\delta_t}{\tau_f + 0.5\delta_t}(f_\alpha^{\mathrm{eq}}(\mathbf{r},t) - \overline{f_\alpha}(\mathbf{r},t)) \tag{1}$$

$$\overline{g_\alpha}(\mathbf{r}+\mathbf{e}_\alpha\delta_t, t+\delta_t) = \overline{g_\alpha}(\mathbf{r},t) + \frac{\delta_t}{\tau_g + 0.5\delta_t}(g_\alpha^{\mathrm{eq}}(\mathbf{r},t) - \overline{g_\alpha}(\mathbf{r},t)) - \frac{\tau_g\delta_t}{\tau_g + 0.5\delta_t} f_\alpha(\mathbf{r},t)h_\alpha(\mathbf{r},t) \tag{2}$$

where

$$\overline{f_\alpha} = f_\alpha + \frac{\delta_t}{2\tau_f}(f_\alpha - f_\alpha^{\mathrm{eq}}) \tag{3}$$

$$\overline{g_\alpha} = g_\alpha + \frac{\delta_t}{2\tau_g}(g_\alpha - g_\alpha^{\mathrm{eq}}) + \frac{\delta_t}{2} f_\alpha h_\alpha \tag{4}$$

$$h_\alpha = (\mathbf{e}_\alpha - \mathbf{u})\cdot\left[-\nabla(P/\rho) + \frac{1}{\rho}\nabla\cdot\prod + (\mathbf{e}_\alpha - \mathbf{u})\cdot\nabla\mathbf{u}\right] \tag{5}$$

and f_α and g_α are the density distribution function and the internal energy density distribution function, respectively; f_α^{eq} and g_α^{eq} are their corresponding equilibrium functions; τ_f and τ_g are the relaxation times of the hydrodynamic and thermodynamic fields, respectively; $\mathbf{r}(x,y,z)$ is coordinate vector, $\mathbf{e}_\alpha$ is the lattice velocity, α is the lattice direction and δ_t is the time interval.

In the study of 3D flow problems, the 3D 15-bit discrete velocity (D3Q15) model [15] is usually used. The equilibrium function f_α^{eq} and g_α^{eq} with the D3Q15 model [14, 15] can be written as

$$f_\alpha^{\mathrm{eq}} = w_\alpha\rho\left[1 + \frac{3\mathbf{e}_\alpha\cdot\mathbf{u}}{c^2} + \frac{9(\mathbf{e}_\alpha\cdot\mathbf{u})^2}{2c^4} - \frac{3\mathbf{u}^2}{2c^2}\right] \tag{6}$$

$$g_\alpha^{\mathrm{eq}} = w_\alpha\rho\varepsilon\left[\frac{3(\mathbf{e}_\alpha^2 - \mathbf{u}^2)}{2c^2} + 3\left(\frac{3\mathbf{e}_\alpha^2}{2c^2} - 1\right)\frac{(\mathbf{e}_\alpha\cdot\mathbf{u})}{c^2} + \frac{9(\mathbf{e}_\alpha\cdot\mathbf{u})^2}{2c^4}\right] \tag{7}$$

where

$$\mathbf{e}_\alpha = \begin{cases} 0, & \alpha = 0 \\ (\pm c,0,0),\ (0,\pm c,0),\ (0,0,\pm c), & \alpha = 1-6 \\ (\pm c,\pm c,\pm c), & \alpha = 7-14 \end{cases} \tag{8}$$

and $c = \sqrt{3RT_0}$ and T_0 is the average temperature. w_α is the weighting coefficient and is $2/9$ for $\alpha = 0$, $1/9$ for $\alpha = 1-6$ and $1/72$ for $\alpha = 7-14$.

In the conventional Boltzmann equation with BGK model, the relaxation time τ_f and τ_g can be linked to the viscosity and thermal conductivity of fluid in such a way that the correct continuity, momentum and energy equations at continuum N–S level are recovered [15, 21] through Chapman–Enskog expansion [26]. However, the above process may not be applicable to the micro flow. This is because the process of recovering the Navier–Stokes level equations implicitly uses continuum assumption, which may not be true for the micro flow. From the kinetic theory [9, 18], we know that the collision frequency in the BGK model can be written as $4P/\pi\mu$ for hydrodynamic field or $2P/5R\kappa$ for thermodynamic field, where μ and κ are the viscosity and thermal conductivity of fluid, respectively. This implies that τ_f and τ_g can be written as

$$\tau_f = \frac{\pi}{4}\frac{\mu}{P} = \frac{\pi}{4}\frac{\mu}{\rho c_s^2} \tag{9}$$

$$\tau_g = \frac{\mu}{\Pr \rho c_s^2} \tag{10}$$

where c_s is the sound speed, $\Pr (= \mu c_p/\kappa)$ is the Prandtl number, c_p $(= \gamma R/(\gamma - 1))$ is specific heat capacity at constant pressure and γ $(= 5/3$ for a monatomic ideal gas and $7/5$ for a diatomic gas) is the heat capacity ratio of gas.

According to kinetic theory, for the hard sphere molecules [9, 13], the Knudsen number can be written as

$$Kn = \sqrt{\frac{\pi\gamma}{2}}\frac{Ma}{Re} \tag{11}$$

where $Re = \rho U_\infty H/\mu$ is the Reynolds number and $Ma = U_\infty/c_s$ is the Mach number. For the D3Q15 model, c_s is taken as $c_s = c/\sqrt{3}$ and c is usually chosen as 1. So, Equation (11) can also be written as

$$Kn = \frac{\pi}{4}\sqrt{\frac{\pi\gamma}{2}}\frac{\mu}{\rho c_s H} \tag{12}$$

By combining Equations (9)–(12), we obtain

$$\tau_f \approx \frac{\pi}{4} H \cdot Kn \tag{13}$$

$$\tau_g \approx \frac{\pi}{4}\frac{H \cdot Kn}{Pr} \tag{14}$$

Equations (13) and (14) are used in the present work to determine the relaxation times once Kn number is given.

The macroscopic density ρ, velocity $\mathbf{u}$, internal energy ε and pressure P can be computed by the conservation laws of mass, momentum, energy and the equation of state

$$\rho = \sum_\alpha \overline{f_\alpha} \quad \rho\mathbf{u} = \sum_\alpha \overline{f_\alpha}\mathbf{e}_\alpha \quad \rho\varepsilon = \sum_\alpha \overline{g_\alpha} - \frac{\delta_t}{2}\sum_\alpha \overline{f_\alpha} h_\alpha \quad P = \frac{2}{D}\rho\varepsilon \tag{15}$$

where $\varepsilon = DRT/2$, T is the temperature and D is the dimension.

The boundary condition is an important issue for LBM simulation in microfluidic systems. Theoretically, the particle–solid interactions should be adequately addressed when the particles

impinge and emerge at solid wall surfaces, and this issue should be traced to the kinetic theory. According to our previous derivation [17], a diffuse scattering boundary condition (DSBC) for the density distribution function f_α and similarly for the internal energy density distribution function g_α in the LBM on any kind of boundary geometries can be constructed as

$$|(\mathbf{e}_\alpha - \mathbf{u}_w) \bullet \mathbf{n}| f_\alpha = \sum_{(\mathbf{e}_{\alpha'} - \mathbf{u}_w) \bullet \mathbf{n} < 0} |(\mathbf{e}_{\alpha'} - \mathbf{u}_w) \bullet \mathbf{n}| \Re_f(\mathbf{e}_{\alpha'} \to \mathbf{e}_\alpha) f_{\alpha'} \tag{16}$$

$$|(\mathbf{e}_\alpha - \mathbf{u}_w) \bullet \mathbf{n}| g_\alpha = \sum_{(\mathbf{e}_{\alpha'} - \mathbf{u}_w) \bullet \mathbf{n} < 0} |(\mathbf{e}_{\alpha'} - \mathbf{u}_w) \bullet \mathbf{n}| \Re_g(\mathbf{e}_{\alpha'} \to \mathbf{e}_\alpha) g_{\alpha'} \tag{17}$$

and

$$\Re_f(\mathbf{e}_{\alpha'} \to \mathbf{e}_\alpha) = \frac{A_N}{\rho_w}((\mathbf{e}_\alpha - \mathbf{u}_w) \bullet \mathbf{n}) f_\alpha^{\mathrm{eq}} \Big|_{\mathbf{u} = \mathbf{u}_w} \tag{18}$$

$$\Re_g(\mathbf{e}_{\alpha'} \to \mathbf{e}_\alpha) = \frac{B_N}{\rho_w \varepsilon}((\mathbf{e}_\alpha - \mathbf{u}_w) \bullet \mathbf{n}) g_\alpha^{\mathrm{eq}} \Big|_{\mathbf{u} = \mathbf{u}_w,\, \varepsilon = \varepsilon_W} \tag{19}$$

where α' and α are directions of the incident and reflected particles, respectively, and A_N and B_N are normalization coefficients which must guarantee no normal flow through the wall and the normal part of the energy flux is continuous. These two coefficients are also dependent on the velocity model used in the LBM.

The inlet boundary conditions in the present study are set at constant velocity, density and temperature. The variables at the outlet of the channel are extrapolated from the values at two neighbouring inner points.

TAYLOR SERIES EXPANSION AND LEAST SQUARE-BASED LATTICE BOLTZMANN METHOD (TLLBM)

The TLLBM developed by Shu *et al.* [21] is based on the standard lattice Boltzmann equation (LBE), the well-known Taylor series expansion, the Runge–Kutta method for solving ordinary differential equations, and the least square optimization. Due to the restriction of the LBE to regular lattice [15], at each time step, the particle described by the LBE may not stream to the neighbouring mesh point if an irregular grid is used in the computation. However, since the particle distribution function is a continuous function in physical space and can be well defined in any mesh system, the Taylor series expansion in space can be used to obtain the value of the distribution functions at corresponding mesh points. The final algebraic formulation of the 3D TLLBM for the density distribution function f_α and the internal energy density distribution function g_α can be written as

$$\overline{f_\alpha}(x_0, y_0, z_0, t + \delta t) = \sum_{k=1}^{N+1} a_\alpha^{1,k} \tilde{f}_\alpha^{k-1} \tag{20a}$$

$$\overline{g_\alpha}(x_0, y_0, z_0, t + \delta t) = \sum_{k=1}^{N+1} a_\alpha^{1,k} \tilde{g}_\alpha^{k-1} \tag{20b}$$

where N is the number of neighbouring mesh points around the reference mesh point (x_0, y_0), $a_\alpha^{1,k}$ are the elements of the first row of the following matrix $[A]$, and

$$[A] = ([S]^{\mathrm{T}}[S])^{-1}[S]^{\mathrm{T}} \tag{21}$$

$[S]$ is a $(N+1) \times 10$ dimensional matrix, which is given as

$$[S] = \begin{bmatrix} 1 & \Delta x_0 & \Delta y_0 & \Delta z_0 & (\Delta x_0)^2/2 & (\Delta y_0)^2/2 & (\Delta z_0)^2/2 & \Delta x_0 \Delta y_0 & \Delta x_0 \Delta z_0 & \Delta y_0 \Delta z_0 \\ 1 & \Delta x_1 & \Delta y_1 & \Delta z_1 & (\Delta x_1)^2/2 & (\Delta y_1)^2/2 & (\Delta z_1)^2/2 & \Delta x_1 \Delta y_1 & \Delta x_1 \Delta z_1 & \Delta y_1 \Delta z_1 \\ - & - & - & - & - & - & - & - & - & - \\ - & - & - & - & - & - & - & - & - & - \\ - & - & - & - & - & - & - & - & - & - \\ 1 & \Delta x_N & \Delta y_N & \Delta z_N & (\Delta x_N)^2/2 & (\Delta y_N)^2/2 & (\Delta z_N)^2/2 & \Delta x_N \Delta y_N & \Delta x_N \Delta z_N & \Delta y_N \Delta z_N \end{bmatrix}_{(N+1)\times 10} \tag{22}$$

where

$$\Delta x_i = x_i + e_{\alpha x}\delta t - x_0, \quad \Delta y_i = y_i + e_{\alpha y}\delta t - y_0, \quad \Delta z_i = z_i + e_{\alpha z}\delta t - z_0$$

$$\tilde{f}_\alpha^k = \overline{f_\alpha}(x_k, y_k, z_k, t) + \frac{\delta_t}{\tau_f + 0.5\delta_t}[f_\alpha^{\mathrm{eq}}(x_k, y_k, z_k, t) - \overline{f_\alpha}(x_k, y_k, z_k, t)]$$

$$\tilde{g}_\alpha^k = \overline{g_\alpha}(x_k, y_k, z_k, t) + \frac{\delta_t}{\tau_g + 0.5\delta_t}[g_\alpha^{\mathrm{eq}}(x_k, y_k, z_k, t) - \overline{g_\alpha}(x_k, y_k, z_k, t)]$$

$$+ \frac{\tau_g \delta_t}{\tau_g + 0.5\delta_t} f_\alpha(x_k, y_k, z_k, t) h_\alpha(x_k, y_k, z_k, t)$$

$$k = 0, 1, \ldots, N$$

Since the coefficients only depend on the coordinates of mesh points and lattice velocity, and are computed in advance, the new method is essentially a meshless method, and can be applied to any lattice velocity model [21].

NUMERICAL SIMULATIONS OF FLOW AND HEAT TRANSFER IN A RECTANGULAR MICROCHANNEL

As illustrations for the present LBM in simulating the flow and heat transfer problems, developing thermal flows in rectangular microchannels with different aspect ratios are simulated. The geometry of the problem is given in Figure 1. The centre of the coordinate system is located at the centre of the channel in the entrance plane. Heat flux at the wall is constant both axially and along the periphery. Initially, the flow is assumed static with a constant temperature T_0. The Reynolds number and the Prandtl number are taken as 0.1 and 0.7, respectively. During simulations, a uniform velocity U_0 and a constant temperature $T_{\mathrm{in}} = T_0$ are

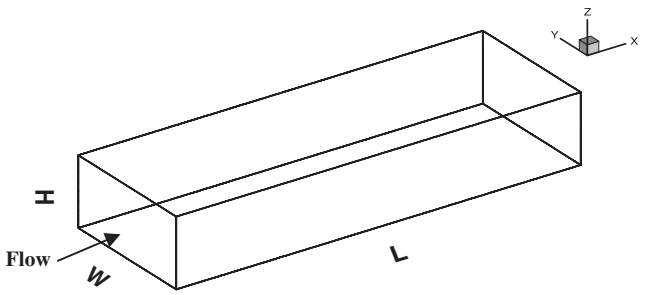

Figure 1. The schematic of flow through the rectangular microchannel.

imposed at the channel inlet and the flow at the outlet is assumed hydrodynamically and thermally fully developed. The DSBC is used on the walls for the density and internal energy density distribution functions. All simulations are based on the non-uniform grids with higher concentration close to the wall and the channel inlet and all results are normalized by the inlet condition unless otherwise mentioned. Since the available data on this problem are very few, the results obtained are only compared with the analytical results of Tunc and Bayazitoglu [24] and the DSMC simulations [25]. In their studies, the traditional momentum and energy equations with the first-order velocity slip and temperature jump boundary conditions are solved using the integral transform technique.

Grid-dependence study

The grid-dependence study based on the case of thermal flows in a channel with aspect ratio of $\beta = H/W = 1$ for inlet Knudsen number of $Kn = 0.04, 0.06$ and 0.08 is first conducted. It should be noted that the lower the aspect ratio β, the more slender the regular cross-section of the duct. In the present computation, W is kept constant and β is varied by changing H, and Kn is always defined in terms of inlet conditions. Three mesh sizes with the same minimum grid stretch ratio of 0.04 in the computational domain are examined and they are $201 \times 13 \times 13$, $201 \times 15 \times 15$ and $201 \times 17 \times 17$ with minimum grid spacings of $0.024, 0.014$ and 0.008, respectively. The results of the grid-dependence study are displayed in Table I in terms of the non-dimensional wall slip velocities U_S and the Nusselt number at the channel outlet. The slip velocity, Nusselt number and friction coefficient are defined as

$$U_S = u_s/u_b \tag{23}$$

$$Nu = \frac{D_h q_{w,m}}{\kappa(T_{w,m} - T_b)} \tag{24}$$

$$C_f = \frac{S_{w,m}}{(1/2)\rho u_b^2} \tag{25}$$

where $u_b = \int_0^W \int_0^H u \, \mathrm{d}y \, \mathrm{d}z / WH$ is the bulk mean velocity; $T_b = \int_0^W \int_0^H \rho u T \, \mathrm{d}y \, \mathrm{d}z / \int_0^W \int_0^H \rho u \, \mathrm{d}y \, \mathrm{d}z$ is the bulk mean temperature; $q_{w,m} = [\int_0^W (\kappa \partial T/\partial z)_w \, \mathrm{d}y + \int_0^H (\kappa \partial T/\partial y)_w \, \mathrm{d}z]/(W + H)$ is the peripheral mean wall heat flux; $T_{w,m} = [\int_0^W T_w \, \mathrm{d}y + \int_0^H T_w \, \mathrm{d}z]/(W + H)$ is the periph-

Table I. The grid-dependence study based on the case of thermal flows in a channel with aspect ratio $\beta = 1$ for different inlet Knudsen numbers at the exit plane of channel.

Mesh	$U_{s-\text{ave}}$	Nu
	$Kn = 0.04$	
$201 \times 13 \times 13$	0.2576	3.09
$201 \times 15 \times 15$	0.2548	3.16
$201 \times 17 \times 17$	0.2551	3.18
	$Kn = 0.06$	
$201 \times 13 \times 13$	0.3207	2.81
$201 \times 15 \times 15$	0.3183	2.87
$201 \times 17 \times 17$	0.3150	2.89
	$Kn = 0.08$	
$201 \times 13 \times 13$	0.3814	2.60
$201 \times 15 \times 15$	0.3742	2.62
$201 \times 17 \times 17$	0.3738	2.62

eral mean wall temperature; and $S_{w,m} = [\int_0^W (\mu \partial u/\partial z)_w \, \mathrm{d}y + \int_0^H (\mu \partial u/\partial y)_w \, \mathrm{d}z]/(W + H)$ is the peripheral mean wall shear stress, respectively; $D_h = 4WH/(2W + 2H)$ is the hydraulic diameter of the channel. As shown in Table I, the difference between the present results on three grid sizes is less than 2%. This indicated that the grid size $201 \times 15 \times 15$ is sufficient for the present LBM to obtain accurate numerical results and hence it is used in the following simulations.

Developing thermal flows in a rectangular channels

Figures 2(a) and (b) shows the velocity and temperature distributions in the microchannel for $\beta = 0.5$ and $Kn = 0.06$. As shown in these figures, the flow becomes quickly fully developed after a short entrance region where the hydrodynamic and thermal boundary layers are developing simultaneously. Because of a larger temperature gradient near the wall, the acceleration near the wall is greater than that at the centre, especially at the entrance region. A more detailed illustration of the flow field in the entrance region for $\beta = 0.5$ and $Kn = 0.06$ is shown in Figures 3(a)–(d) and 4(a)–(d), where the dimensionless x-component velocity and temperature profiles at different positions along the channel are plotted. From Figures 3(a)–(d) and 4(a)–(d), obvious velocity slips and temperature slips at the walls are observed because of the rarefaction effects. They also indicate that the flow is fully developed within a distance less than the width of the channel.

To verify the accuracy of the present method, we compare the velocity profiles along the horizontal and vertical centrelines of the cross-section at the exit of the channel between the present simulations, the analytical solution based N–S equations [24] and the DSMC simulations [25] in Figures 5(a) and (b) for the cases of $Kn = 0.05$ and $\beta = 0.2$. The Kn and β were chosen to match the available published results for comparison although in the present study, we focus on $Kn = 0.04, 0.06, 0.08$. As shown in Figure 5, the results obtained by different approaches agree well with each other.

The variation of average friction coefficients and Nusselt numbers at channel outlet with respect to the aspect ratio for different inlet Knudsen numbers are given in Figures 6(a)

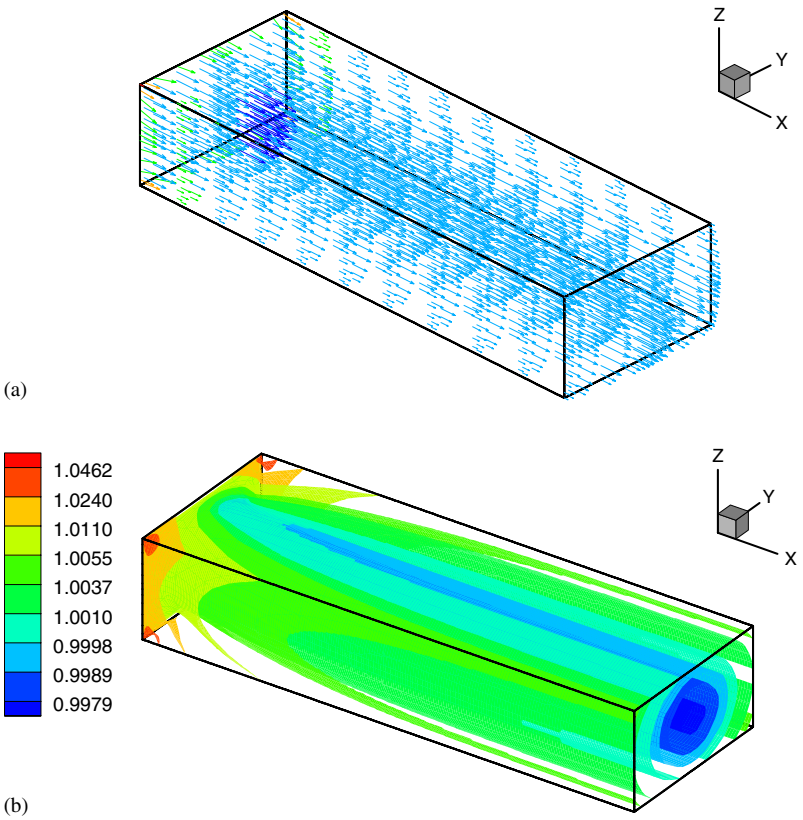

Figure 2. Velocity and temperature distributions in the microchannel for $\beta = 0.5$ and $Kn = 0.06$: (a) velocity distribution along the channel; and (b) temperature distribution in the channel.

and (b). For the same aspect ratio, the friction coefficient decreases with increasing inlet Knudsen number. This trend is reasonable since the flow is more rarefied at higher Knudsen number. For the same Knudsen number, the friction coefficient decreases as the aspect ratio becomes smaller, i.e. the channel becomes slender. This can be explained in term of the reduced slip velocity at the corner as indicated in Figure 3. When the channel becomes slender, the larger slip velocity region in the middle section of z direction decreases. In this region, the velocity gradient in the y direction is large and hence the contribution to skin friction stress is high. A reduction in this middle section region in the z direction would result in overall reduction in skin friction coefficient. Regardless of the value of the aspect ratio, the Nusselt number always decreases when Kn increases. Again it is reasonable to expect a lower convective heat transfer rate due to rarefaction effect at higher Knudsen number. The Nusselt number also decreases with decreasing aspect ratio. This can also be explained in term of reduced temperature slip at the corner as indicated in Figure 4 in a similar way as that for reduced friction coefficient. When the channel becomes slender, the larger slip temperature region in the middle section of z direction decreases. In this region, the temperature gradient

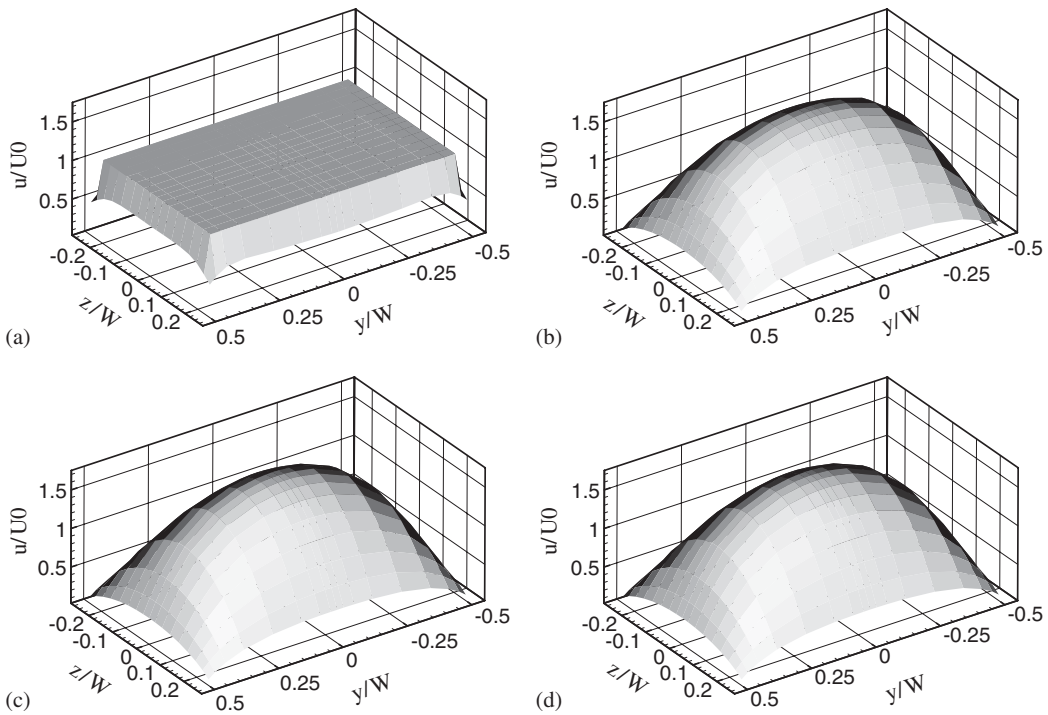

Figure 3. Dimensionless velocity profiles at the entrance region of the microchannel for $\beta = 0.5$ and $Kn = 0.06$: (a) $x/W = 0.0$; (b) $x/W = 0.3442$; (c) $x/W = 0.7826$; and (d) $x/W = 1.230$.

in the y direction is large and hence the contribution to heat transfer is high. A reduction in this middle section region in the z direction would result in overall reduction in heat transfer and hence Nusselt number.

The most interesting phenomenon observed in Figure 6 is that the trend of variation of the friction coefficients with aspect ratio in the micro channel flow is completely different from that of the non-slip macro-channel flow [27]. Although it is expected that the rarefied flow will have a lower friction coefficient than that for continuum flow, the opposite in trend of variation with aspect ratio is intriguing. The above observations can be explained in term of non-slip velocity condition at the wall for continuum flow. As explained before, the decrease in skin friction coefficient when the flow channel become slender is due to the variation of slip velocity at the wall. Such variation cannot occur in continuum flow as the slip velocity is zero. It is noted that for continuum flow, the friction stress at corner flow region is relatively smaller due to lower velocity there. This has been the inspiration for the introduction of riblet device to reduce skin friction stress in boundary layer flow. For very slender channel, the flow becomes almost two-dimensional similar to that between two flat infinite plates. Thus it is natural to expect that the corner flow effect is reduced and the friction coefficient increases as the channel becomes slender. The present results clearly indicate the inadequacy of the continuum assumption in Navier–Stokes solvers for micro-channel flows as it not only

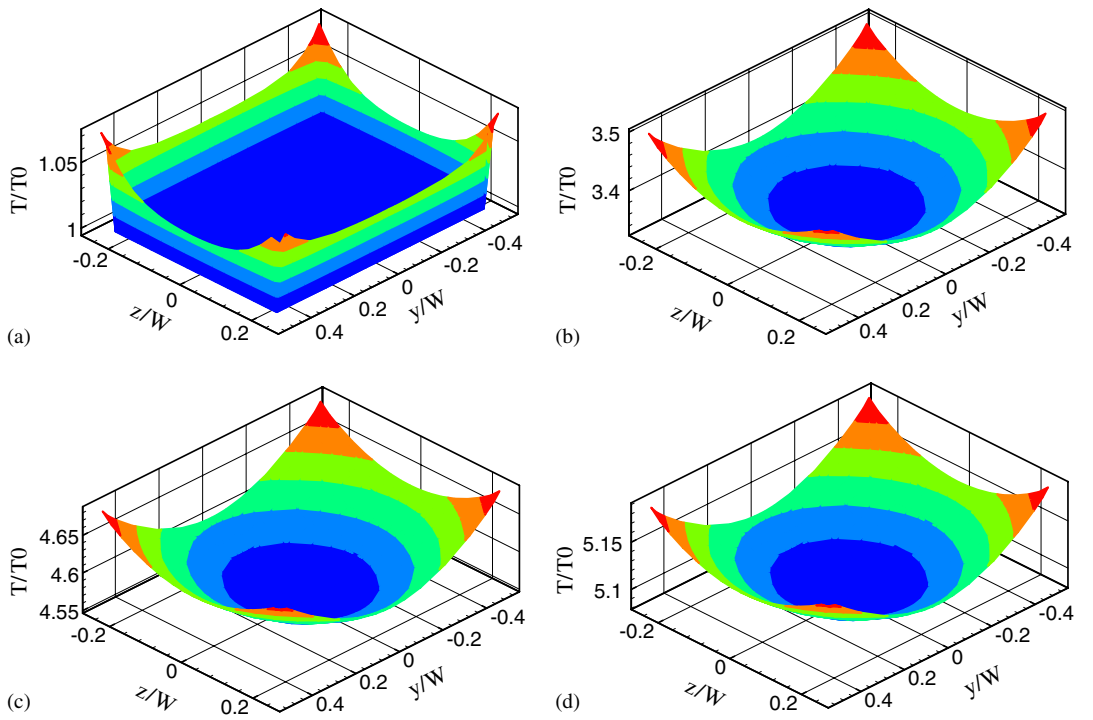

Figure 4. Dimensionless temperature profiles at the entrance region of the microchannel for $\beta = 0.5$ and $Kn = 0.06$: (a) $x/W = 0.0$; (b) $x/W = 0.3442$; (c) $x/W = 0.7826$; and (d) $x/W = 1.230$.

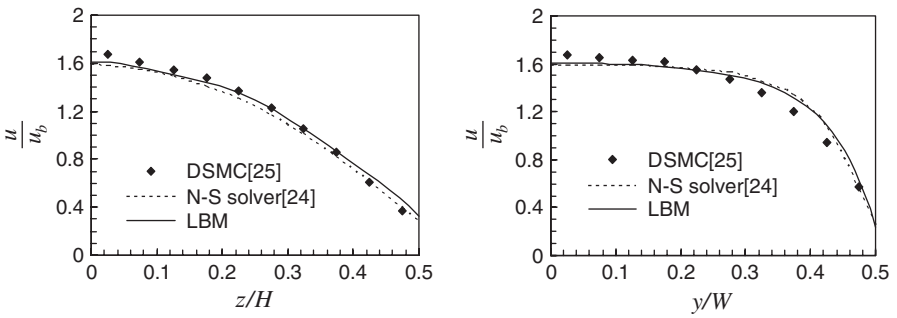

Figure 5. Comparison of the velocity profiles of the centrelines of the cross-section at the exit of the channel between different approaches for $Kn = 0.05$, $\beta = 0.2$.

predicts the magnitude of friction coefficient wrongly, but also its trend of variation with aspect ratio.

Table II compares the slip velocity and the Nusselt numbers obtained by our simulations with those of Tunc and Bayazitoglu [24] at the mid width W of wall in the exit plane of channel. As shown in this table, the slip velocities obtained by our simulations are close to the

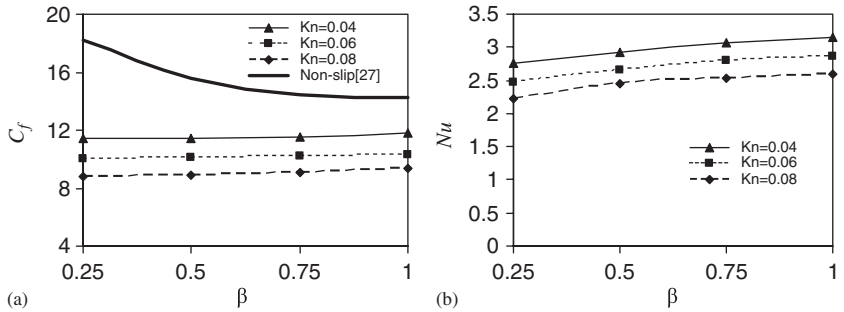

Figure 6. The variation of the friction coefficient and Nusselt number with respect to the aspect ratio for different inlet Knudsen numbers: (a) friction coefficient; and (b) Nusselt number.

Table II. Comparisons of the slip velocity and the Nusselt numbers obtained by present simulations and those of Tunc and Bayazitoglu [24] at the mid width W of wall in the exit plane of channel.

	U_s		Nu	
β	Reference [24]	Present	Reference [24]	Present
		$Kn = 0.04$		
1	0.21	0.25	2.85	3.16
0.75	0.25	0.27	2.81	3.06
0.5	0.32	0.30	2.71	2.92
		$Kn = 0.06$		
1	0.28	0.31	2.69	2.87
0.75	0.33	0.33	2.62	2.79
0.5	0.41	0.36	2.48	2.66
		$Kn = 0.08$		
1	0.34	0.37	2.53	2.60
0.75	0.39	0.38	2.44	2.54
0.5	0.48	0.41	2.26	2.44

analytical results of Tunc and Bayazitoglu while the Nusselt numbers obtained by the present method are larger than those of Tunc and Bayazitoglu. The deviations between our simulations and the work of Tunc and Bayazitoglu may be attributed to the insufficient consideration of the rarefactions in the analysis of Tunc and Bayazitoglu, in which the rarefaction effects are only considered on the wall boundaries. This resulted in their slip velocities and temperatures being constant along the x direction. It is rather difficult to expect this since the rarefaction effect varies along the channel length.

CONCLUSIONS

A 3D lattice Boltzmann BGK model for micro flow and heat transfer had been presented based on kinetic theory considerations and the thermal lattice Boltzmann method. The kinetic relations of the relaxation times were redefined and linked with the Knudsen number. A diffuse scattering boundary condition (DSBC) for the velocity and thermal fields was presented for the 3D LBM. The present 3D lattice Boltzmann model was successfully applied to simulate the flow and heat transfer in rectangular micro-channels using our 3D TLLBM. Numerical simulation shows that the LBM can give a good prediction of the micro fluidic behaviours with thermal effects, and clearly indicate the inadequacy of the continuum assumption in Navier–Stokes solvers for micro-channel flows.

REFERENCES

1. Mudawar I. Assessment of high-heat-flux thermal management schemes. *Proceedings of the Seventh Intersociety Conference on Thermal and Thermomechanical Phenomena in Electronic Systems*, vol. 1, 2000; 1.
2. Yeh LT. Review of heat transfer technologies in electronic equipment. *ASME Journal of Electronic Packaging* 1995; **117**:333–337.
3. Tuckerman DB, Pease RFW. High-performance heat sinking for VLSI. *IEEE Electron Device Letters* 1981; **EDL-2**:126–129.
4. Wu PY, Little WA. Measurement of the heat transfer characteristics of gas flow in fine channel heat exchangers for micro miniature refrigerators. *Cryogenics* 1984; **24**:415–420.
5. Peng XF, Peterson GP, Wang BX. Heat transfer characteristics of water flowing through microchannels. *Experimental Heat Transfer* 1994; **7**:265–283.
6. Yang C, Li D, Masliyah JH. Modeling forced liquid convection in rectangular microchannels with electrokinetics effects. *International Journal of Heat and Mass Transfer* 1998; **41**:4229–4249.
7. Samalam VK. Convective heat transfer in microchannels. *Journal of Electronic Materials* 1989; **18**:611–618.
8. Qu W, Mudawar I. Analysis of three-dimensional heat transfer in micro-channel heat sinks. *International Journal of Heat and Mass Transfer* 2002; **45**:3973–3985.
9. Sharipov F, Seleznev V. Data on internal rarefied gas flows. *Journal of Physical and Chemical Reference Data* 1998; **27**(3):657–706.
10. Loyalka SK, Hamoodi SA. Poiseuille flow of a rarefied gas in a cylindrical tube: solution of linearized Boltzmann equation. *Physics of Fluids A* 1990; **2**(11):2061–2065.
11. Ohwada T, Sone Y, Aoki K. Numerical analysis of the Poiseuille and thermal transpiration flows between two parallel plates on the basis of the Boltzmann equation for hard sphere molecules. *Physics of Fluids A* 1989; **1**(12):2042–2049.
12. Koplik J, Banavar JR. Continuum deductions from molecular hydrodynamics. *Annual Review of Fluid Mechanics* 1995; **27**:257–292.
13. Bird G. *Molecular Gas Dynamics and the Direct Simulation of Gas Flows*. Oxford Science Publications: Oxford, 1994.
14. Benzi R, Succi S, Vergassola M. The lattice Boltzmann equation: theory and applications. *Physics Reports—Review Section of Physics Letters* 1992; **222**:145–197.
15. Chen S, Doolen GD. Lattice Boltzmann method for fluid flows. *Annual Review of Fluid Mechanics* 1998; **30**:329–364.
16. Bhatnagar PL, Gross EP, Krook M. A model for collision processes in gases. I. Small amplitude processes in charged and neutral one-component systems. *Physical Review* 1954; **94**:511–525.
17. Niu XD, Shu C, Chew YT. A lattice Boltzmann BGK model for simulation of micro flows. *Europhysics Letters* 2004; **67**(4):600–606.
18. Cercignani C. *Mathematical Methods in Kinetic Theory*. Plenum: New York, 1969.
19. He X, Chen S, Doolen GD. A novel thermal model for the lattice Boltzmann method in incompressible limit. *Journal of Computational Physics* 1998; **146**:282–300.
20. Karniadakis GE, Beskok A. *Micro Flows*: *Fundamentals and Simulation*. Springer: New York, 2002.
21. Shu C, Chew YT, Niu XD. Least square-based LBM: a meshless approach for simulation of flows with complex geometry. *Physical Review E* 2001; **64** 045701:1–4.
22. Shu C, Niu XD, Chew YT. Taylor series expansion- and least square-based lattice Boltzmann method: two-dimensional formulation and its applications. *Physical Review E* 2002; **65** 036708:1–13.

23. Chew YT, Shu C, Niu XD. Simulation of unsteady incompressible flows by using Taylor series expansion- and least square-based lattice Boltzmann method. *International Journal of Modern Physics C* 2002; **13**(6):719–738.
24. Tunc G, Bayazitoglu Y. Heat transfer in rectangular microchannels. *International Journal of Heat and Mass Transfer* 2002; **45**:765–773.
25. Mao XH. Private communication.
26. Chapman S, Cowling T. *Mathematical Theory of Non-uniform Gases* (3rd edn). Cambridge University Press: London, 1970.
27. Shah RK, London AL. *Laminar Flow Forced Convection in Ducts*. Academic Press: London, 1978.

